COMMUNICATION

Check for updates

Photopolymerized superhydrophobic hybrid coating enabled by dual-purpose tetrapodal ZnO for liquid/liquid separation†

Chenxuan Li, [ID] [a] Brian Lee, [a] Chenxu Wang, [ID] [b] Aayushi Bajpayee, [ab]
Lacey D. Douglas, [ab] Bailey K. Phillips, [a] Guanghua Yu, [ab] Natalia Rivera-Gonzalez, [ab]
Bo-ji Peng, [a] Zhiyuan Jiang, [b] Hung-Jue Sue, [ID] [b] Sarbajit Banerjee [ID] ★[ab] and
Lei Fang [ID] ★[ab]

Low-cost and scalable superhydrophobic coating methods provide viable approaches for energy-efficient separation of immiscible liquid/liquid mixtures. A scalable photopolymerization method is developed to functionalize porous substrates with a hybrid coating of tetrapodal ZnO (T-ZnO) and polymethacrylate, which exhibits simultaneous superhydrophobicity and superoleophilicity. Here, T-ZnO serves dual purposes by (i) initiating radical photopolymerization during the fabrication process through a hole-mediated pathway and (ii) providing a hierarchical surface roughness to amplify wettability characteristics and suspend liquid droplets in the metastable Cassie—Baxter regime. Photopolymerization provides a means to finely control the conversion and spatial distribution of the formed polymer, whilst allowing for facile large-area fabrication and potential coating on heat-sensitive substrates. Coated stainless-steel meshes and filter papers with desired superhydrophobic/superoleophilic properties exhibit excellent performance in separating stratified oil/water, oil/ionic-liquid, and water/ionic-liquid mixtures as well as water-in-oil emulsions. The hybrid coating demonstrates desired mechanical robustness and chemical resistance for their long-term application in large-scale energy-efficient separation of immiscible liquid/liquid mixtures.

New concepts

In this manuscript, we report a conceptually new approach to photochemically fabricate orthogonally wettable hybrid coating materials by exploiting the dual functions of tetrapodal ZnO (T-ZnO): photoinitiating radical polymerization, and imbuing hierarchical multiscale surface roughness to amplify wettability characteristics. Through this new concept, the challenges associated with the scalable fabrication of coating materials with precisely tunable wettability, such as the need for multiple components, complex and harsh procedures, or high energy consumption, are simultaneously mitigated. The dual role of ZnO tetrapods as photoinitiators and integral textural elements enables the scalable fabrication of polymer/T-ZnO hybrid coatings on stainless steel meshes and on quantitative filter papers. The resulting coating material possesses orthogonal superhydrophobic/superoleophilic surface properties, enabling efficient liquid/liquid separation. The prepared membranes show an unprecedented combination of fabrication feasibility, robustness of function, and ability to effectively engender separations along a surface tension gradient. This work promises broad impacts on materials science by (i) bringing the concept of employing a dual-purpose metal oxide for photochemical coatings; and (ii) enabling highly efficient and large scale liquid/liquid separation for important industrial applications.

Introduction

Large volumes of immiscible mixtures of organic solvents and water are discharged into ecosystems during the extraction of natural resources and as effluents from industrial processes. Oily waste generated in petroleum,[1] mining,[2] and food industries,[3] which can be classified as produced water, rag oil, or slop oil

depending on the water/oil ratio, represents a major concern to the sustainability of these industries.[4] Separation and productive utilization of hydrocarbons from such oily waste requires the removal of aqueous fractions. Furthermore, produced water effluents discharged into water bodies without treatment pose a substantial threat to ecosystems and human health.[5,6] As such, there is an urgent need to develop methods to separate oils from waste water. In addition to conventional oil/water mixtures, ionic liquids (ILs) have also emerged as one of the components in many immiscible liquid mixtures produced in industry. Their increasing use in industrial processes stems from their categorization as "green solvents" as a result of their low vapor pressure.[7,8] Although the separation of immiscible mixtures of oil/water, IL/water, and IL/oil are often straightforward because of their phase-separated nature, conventional approaches such

[a] *Department of Chemistry, Texas A&M University, 3255 TAMU, College Station, TX 77843, USA. E-mail: banerjee@chem.tamu.edu, fang@chem.tamu.edu*

[b] *Department of Materials Science & Engineering, Texas A&M University, 3003 TAMU, College Station, TX 77843, USA*

† Electronic supplementary information (ESI) available. See DOI: 10.1039/d1mh01672e

as gravity settling,[9] centrifugation[10] and electrochemical[11] technologies are plagued by low efficiencies and high cost and incur considerable energy consumption. Therefore, the development of scalable and highly efficient techniques to separate immiscible liquid mixtures has received much recent attention.[12–14]

Materials featuring simultaneous superhydrophobicity ("dislike for water") and superoleophilicity ("affinity for oil") exhibit outstanding selectivity and efficiency[15] for oil/water separation on account of their entirely orthogonal affinities to liquids with high and low surface tension. In order to obtain the desired superwettability, it is essential to impart the materials with (i) a low-surface-energy and (ii) high surface roughness spanning nano-, micro-, and mesoscopic scales to suspend liquid droplets in a Cassie—Baxter regime.[16,17] Strategies to fabricate low-surface-energy composites include electrospinning,[18–20] chemical vapor deposition[21–23] and thermal polymerization.[24–26] Meanwhile, various methods have been developed to fabricate surfaces exhibiting hierarchical surface roughness. These include sol–gel processes,[18,27,28] hydrothermal methods,[19,29] surface etching,[30,31] and microphase separation.[20] Integration of these two types of strategies can impart superhydrophobicity and superoleophilicity onto the material surface. However, most of these fabrication methods either rely on complicated procedures or require high heat input. Currently, it is urgently desired, yet challenging to develop, cost-effective and sustainable methods[32] to fabricate superhydrophobic/superoleophilic materials for large-scale applications.

Tetrapodal zinc oxide (T-ZnO) with cone-like arms spanning micrometers in length and tapering to nanometer-sized tips is a promising material for the construction of superwettable surfaces as a result of its ability to imbue multiscale roughness to surfaces because of its distinctive three-dimensional geometry.[33] ZnO is also a suitable material for large scale applications owing to its nontoxicity and low cost. Initially, T-ZnO was directly coated onto the surface with no binder.[34] Although superhydrophobicity was achieved, the poor chemical stability and non-adhesive nature of the powder-like coating materials hampered practical applications. We have previously reported the enhanced mechanical resilience of T-ZnO coating materials by incorporating a silica coating layer.[35–37] Recently, Yamauchi and coworkers utilized[38] a hybrid of polydimethylsiloxane (PDMS)[38–40] and T-ZnO to afford a durable and flexible superhydrophobic surface. Nevertheless, these methods require either continuous high heating that is problematic for large scale production, and/or the addition of catalyst that could lead to significant increase in cost.

In this work, we describe a cost-effective and scalable photopolymerization approach for the fabrication of a superwettable composite of polymer and T-ZnO. It is particularly attractive because ZnO is also known[41–45] to be an efficient, non-migratable photoinitiator of radicals. Nevertheless, only a few examples have been reported on the synthesis of functional ZnO/polymer composites through ZnO-promoted photopolymerization.[27,46] We envisioned that T-ZnO can potentially serve dual purposes by (i) imbuing multiscale surface roughness and (ii) initiating spatially controlled photopolymerization for the

synthesis of polymer binder. Herein, by taking the advantage of dual-purpose T-ZnO, we report a feasible and scalable photochemical method to fabricate a superhydrophobic/superoleophilic hybrid coating on meshes for efficient and durable liquid/liquid separation.

Results and discussion

To achieve a superhydrophobic surface with a high water contact angle, hierarchical roughness at multiple scales is required to hinder the transition of a droplet from the Cassie—Baxter state to the Wenzel state.[47] Therefore, we applied T-ZnO with protruding arms of 1–100 μm in length and <1 μm in diameter, synthesized by a previously reported method involving facile and scalable rapid air oxidation of Zn foils, to a stainless steel mesh substrate.[35] Furthermore, we chose radical photopolymerization to construct the polymer adhesive layer by considering the following advantages. First, photoreactions are cost-effective, efficient in energy usage, and feasible for large-scale production. Second, the presence of ZnO as the photoinitiator enables facile photopolymerization without the addition of small molecular photoinitiator, which impose potential issues such as the migration of reacted fragments and unreacted photoinitiators, posing a threat to human health.[48] Finally, photopolymerization can be triggered selectively on the interface of T-ZnO and the monomer solution, giving excellent spatial control of the desired hybrid coating. Various polymer-coated ZnO nanoparticles (ZnONPs) have been reported utilizing this strategy.[46,49,50] Here we leveraged this surface-initiating process to construct the ZnO/polymer hybrid coating with a conformal polymer layer of the desired thickness, avoiding the formation of undesired thick polymer layer on top of ZnO. Polymethacrylates were selected as the polymer component on account of their low cost, feasibility for radical polymerization, and well-established applications as functional coating materials.[51–54]

Fig. 1 illustrates the preparation of T-ZnO/polymethacrylate composite on stainless-steel mesh via ZnO-initiated photopolymerization. T-ZnO was first dispersed in 2-propanol (IPA) and spray-coated onto a clean stainless-steel mesh. Next, the coated mesh was soaked in an IPA solution of a methacrylate monomer [methyl methacrylate (MMA), butyl methacrylate (BMA), or lauryl methacrylate (LMA)]. Subsequently, UV light was applied to the mesh to trigger photopolymerization and hence growth of a layer of polymer on the interface of T-ZnO and solution, followed by washing with methanol and drying. This feasible, low-cost, and energy-efficient procedure allows for fabrication of the hybrid coating in a large scale (example: 25 cm × 25 cm in the laboratory). In the photopolymerization step, several key reaction parameters were investigated to correlate with the reaction efficiency and the superwettability performance. These include solvent, monomer, reaction time, and morphology of ZnO (tetrapodal versus nanoparticle). Monomer conversion of each reaction was analyzed by ^{1}H nuclear magnetic resonance spectra (NMR, Fig. S2–S4, ESI†). Weight fractions of the polymer in the ZnO/polymer composites were
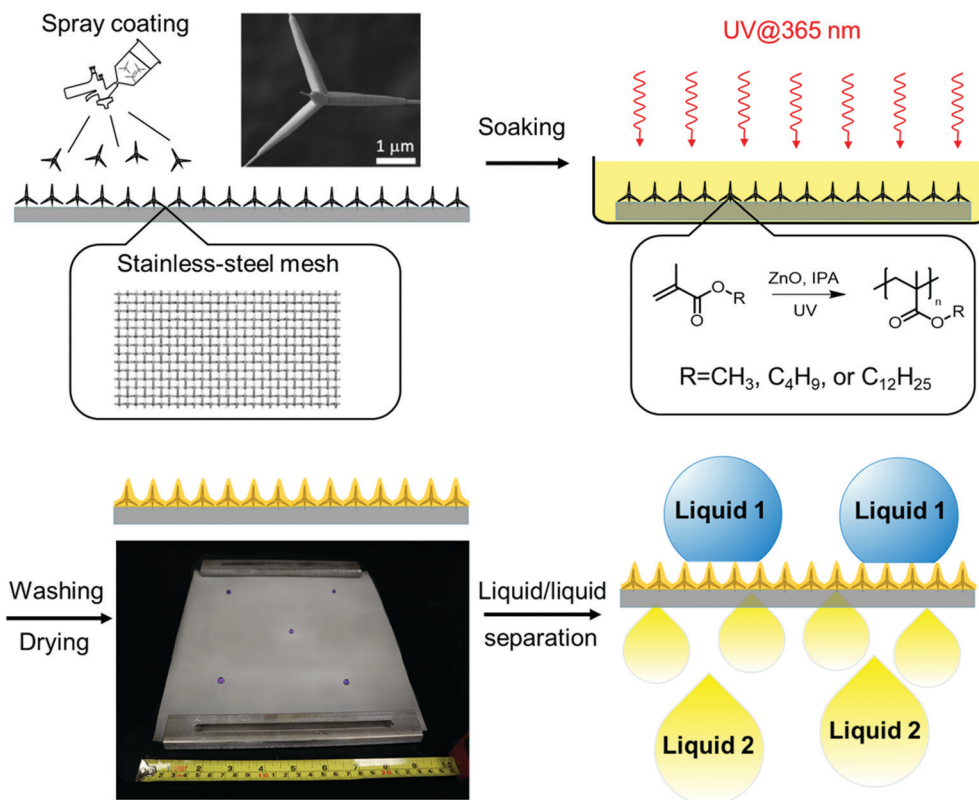
Fig. 1 Schematic representation of the preparation of T–ZnO/polymer hybrid-coated mesh through ZnO-initiated photopolymerization, and its application for liquid/liquid separation. A fully coated 25 cm × 25 cm mesh is shown as an example in the photo.

measured by thermogravimetric analysis (TGA, Fig. S5, ESI†). Number-average molar mass (M_n) and dispersity ($Đ$) of polymers were obtained from size exclusion chromatography (SEC, Fig. S6–S10, ESI†). The results of representative trials are summarized in Table 1.

The monomer conversion is dependent on the presence of ZnO, solvent, and reaction time. In a control experiment without ZnO (Table 1, entries 1 and 2), the photopolymerization required a much longer induction time (>3 h) and gave a low conversion of 10% after 6 h, likely due to the presence of MEHQ inhibitor in the commercial methacrylate starting material and dissolved oxygen that quench radicals formed under UV irradiation. In contrast, with either T-ZnO (Table 1, entries 4–6) or ZnONPs ($d \approx 500$ nm,

determined by dynamic light scattering, Fig. S10, ESI†) (Table 1, entry 8) coated on the mesh, the induction times were both significantly decreased. In the case of T-ZnO, photopolymerization could be initiated within 1 h; a significantly higher conversion was observed after 6 h (39%), confirming the critical function of T-ZnO as a photoinitiator. Furthermore, the polymers formed in the presence of ZnO generally exhibited lower M_n, indicating the generation of more photo-initiated radical chains promoted by ZnO.

Previous studies[41,42] revealed that a protic solvent is often essential in the initiation process of metal–oxide-promoted photopolymerization. Indeed, here a control experiment without the addition of IPA solvent showed no conversion of the

Table 1 Results of thin film photopolymerization

Entry	Type of ZnO	Irradiation time (h)	Monomer	Solvent	Conversion (%)	Weight fraction of polymer (%)	M_n (kDa)	$Đ$	WCA (°)	WSA (°)
1	N/A	3	LMA	IPA	0	N/A	N/A	N/A	111.1	N/A
2	N/A	6	LMA	IPA	10	N/A	174.8	1.92	100.4[a]	N/A
3	T-ZnO	6	LMA	N/A	0	N/A	N/A	N/A	153.1	14
4	T-ZnO	1	LMA	IPA	2	16	95.6	2.46	158.3	7
5	T-ZnO	2	LMA	IPA	5	40	79.9	2.68	155.1	8
6	T-ZnO	4	LMA	IPA	9	60	69.9	3.14	148.1	33
7	T-ZnO	6	LMA	IPA	39	90	40.7	3.67	120.3	N/A
8	ZnONP	2	LMA	IPA	8	26	85.2	3.05	154.0	22
9	T-ZnO	1.5	MMA	IPA	15	40	13.4	2.17	144.5	40
10	T-ZnO	2	BMA	IPA	9	40	26.7	2.49	150.1	28

[a] Contact angle measured on a flat polymer-coated glass substrate.

methacrylate monomer, confirming the important role of protic solvents in the photopolymerization process (Table 1, entry 3). To further ascertain the role of IPA in this reaction, electron paramagnetic resonance studies were carried out on the T-ZnO dispersion in IPA with 5,5-dimethyl-1-pyrroline N-oxide (DMPO) as the radical trapping agent. After UV irradiation, a set of characteristic peaks with a 1:1:1:1:1:1 ratio was detected (Fig. S12, ESI†). The hyperfine splitting pattern and g factor match well with the signals of the DMPO adduct of 2-hydroxy-2-methylethyl radical (Table S1, ESI†).[55] Therefore, the initiation mechanism likely proceeds through a hole pathway (Fig. S13, ESI†). Photogenerated holes in the valence band of ZnO first oxidize surface-adsorbed IPA to generate 2-hydroxy-2-methylethyl radicals, which in turn initiate the free radical polymerization of adjacent methacrylate monomers on the interface of T-ZnO and the solution.

A series of stainless-steel meshes coated with varied hybrid materials were fabricated and investigated in this work. These samples are labeled as "Type of ZnO/Type of polymer-wt% of polymer fraction". For example, "T-ZnO/PLMA-40" represents a stainless-steel mesh sample coated by T-ZnO and poly(lauryl methacrylate) hybrid with a polymer weight fraction of 40%. According to the Cassie—Baxter equation, the intrinsic surface wettability can be greatly amplified by the surface roughness, and thus low surface energy is a must for a superhydrophobic surface. In this work, the intrinsic surface energy was tailored by the chemical composition of the polymer, by simply varying the methacrylate monomers with different alkyl groups. We first investigated the intrinsic surface energy of poly(methyl methacrylate) (PMMA), poly(butyl methacrylate) (PBMA) and poly(lauryl methacrylate) (PLMA) by measuring the static water contact angle (WCA) on each smooth polymer coated on a flat glass substrate (Fig. S14, ESI†). It was found that PLMA with the longest carbon chain exhibited the highest WCA (100.4°), compared to the slightly more hydrophilic surfaces of PBMA (93.9°) and PMMA (73.1°). Subsequently, the surface wettability of T-ZnO/PMMA-40, T-ZnO/PBMA-40, and T-ZnO/PLMA-40 samples was evaluated. The polymer contents in all the samples are kept at 40 wt% in order to maintain similar surface morphology (Fig. S15, ESI†). Notably, the mesh coated with T-ZnO/PMMA-40 showed a WCA of 144.5° ± 4.0° (Fig. 2a) although a smooth PMMA surface is considered weakly hydrophilic. This is in good agreement with the recently reported 65° threshold WCA of smooth surface for achieving amplified hydrophobicity due to the increased fraction of air–liquid interface in the Cassie—Baxter state.[56] T-ZnO/PBMA-40 and T-ZnO/PLMA-40 meshes exhibited higher WCA of 150.0° ± 5.4° and 155.1 ± 1.9°, respectively, which is in line with the trend of more hydrophobic nature of PBMA to PLMA. The T-ZnO/PLMA-40 sample, also with a low water sliding angle (WSA) of 8°, was qualified as being superhydrophobic for oil/water separation. Consequently, PLMA was chosen as the polymer component with a view towards engineering liquid/liquid separations.

The proportion of polymer coated on T-ZnO also influences the surface wettability. Conformal coverage of the T-ZnO by PLMA that traces the contours of the ZnO tetrapods helps to enhance the superhydrophobicity by decreasing the surface free energy. However, an excessive amount of polymer can bury the rough feature of T-ZnO spikes and increase the areal dimensions of solid/liquid contact, thereby destabilizing the Cassie—Baxter state. The convenient photopolymerization approach allowed for feasible control of the amount of polymer formation on T-ZnO/solution interfaces. By simply tuning the UV irradiation time, we prepared T-ZnO/polymer hybrid meshes with varying PLMA content (0–90 wt%) and tested their wettability using DI water as the probe liquid (Fig. 2b). The bare sample with no polymer but only T-ZnO (T-ZnO/PLMA-0) was
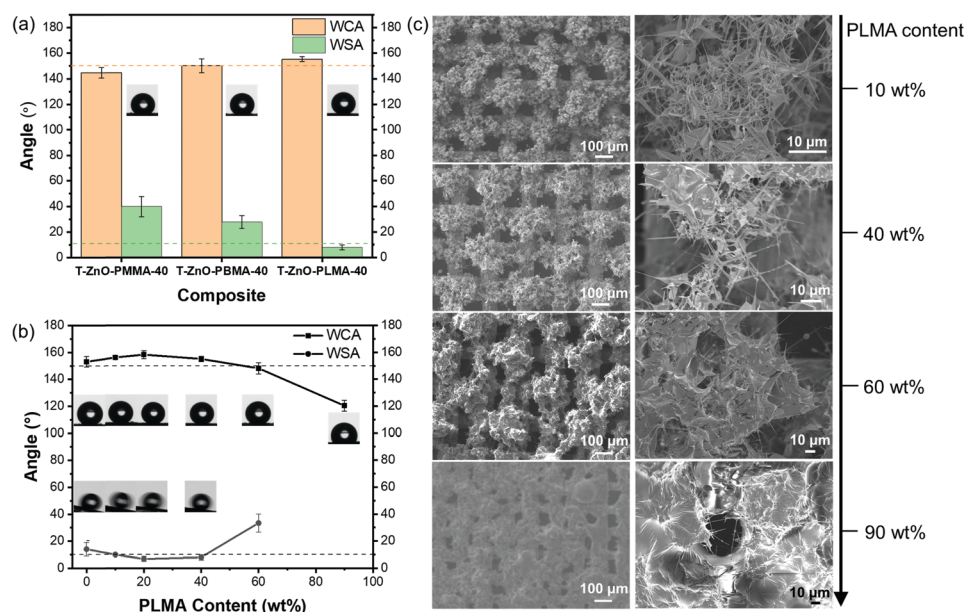

Fig. 2 Wettability of T–ZnO/polymer hybrid meshes with different (a) polymers and (b) PLMA content; (c) SEM images of T–ZnO/polymer hybrid meshes with varied PLMA content.

superhydrophilic owing to the kinetically favorable water adsorption by surface oxygen vacancies on T-ZnO.[29] After drying at 100 °C overnight and stored in the air for a week, its surface wettability was converted, to give a WCA of around 153.1°. With PLMA content ranging from 10% to 40%, the samples T-ZnO/PLMA-10–T-ZnO/PLMA-40 were all superhydrophobic, suggesting the enhanced hydrophobicity raised by the lower surface energy of PLMA. However, with polymer content higher than 40%, the water repellency dropped and WCA decreased, as the hypothesized effect of morphological change. This effect can be clearly observed in the SEM images (Fig. 2c) of T-ZnO/PLMA-10, -40, -60, and -90 samples. For the former two samples, the PLMA component is evenly dispersed in the porous T-ZnO network, connecting the individual T-ZnO without covering the surface. For the samples with 60% and 90% PLMA, however, the T-ZnO spikes are buried by the polymer, thereby diminishing the density of plastronic air pockets and increasing the solid/liquid interfacial contact area. Hence, although more polymer content can potentially enhance adhesion and mechanical robustness of the hybrid, excessive amount of polymer can negatively impact the desired superhydrophobicity. An optimized 40 wt% of PLMA was used in this work for further investigations.

Subsequently, we investigated the essential role that T-ZnO's tetrapodal morphology was playing on the surface wettability. By replacing T-ZnO with ZnONPs, the ZnONP/PLMA-26 sample exhibited a slightly decreased WCA to $153.1° \pm 3.8°$, and a significantly higher WSA of $\sim 22°$ (Table 1, entry 8), confirming the key contribution of T-ZnO to the superhydrophobicity. The broad size distribution of T-ZnO (1–100 μm) and random orientation of these tetrapods rendered a hierarchical surface texturation at microscale and nanoscale. Besides, the typical size of T-ZnO is much larger than ZnONPs (Fig. S16, ESI†). Therefore, dual-scale roughness[47] and relatively greater length[57] helped to keep the liquid-air interface under the droplet by increasing the potential energy barrier separating the Cassie–Baxter state from the Wenzel state. In other words, the size

distribution and tetrapodal shape of T-ZnO ensured the high WCA and low WSA of the hybrid coating.

With the aforementioned data, T-ZnO/PLMA-40 stood out as the most promising coated mesh for liquid/liquid separation. The contact angles of liquids with varied surface tensions on this sample were studied (Fig. 3a), in comparison to those on flat smooth PLMA[58] (Fig. 3b). As expected, the high surface roughness of T-ZnO/PLMA-40 significantly amplified the intrinsic wettability of PLMA toward these liquids. For liquids with high surface tension, T-ZnO/PLMA-40 surface turned drastically more lyophobic compared to smooth PLMA. The contact angles of water, 1-Butyl-3-methylimidazolium tetrafluoroborate ([Bmim][BF$_4$]) and 25 wt% ethanol/water solution were increased from $\sim 100.4°$, 96.5° and 77.4° to $\sim 155.1°$, 147.8° and 124.0°, respectively. For low surface tension liquids, 30 wt% ethanol–water solution, 1-hexyl-3-methylimidazolium bis(trifluoromethyl-sulfonyl)imide ([Hmim][TFSI]) and hexadecane droplets were in more intimate contact with T-ZnO modified composite ($\sim 39.0°$, 37.7° and 0°, respectively) compared to that on the smooth PLMA surface ($\sim 67.6°$, 63.5° and 23.4°, respectively); and were able to spread on the membrane in a short time. This phenomenon is in good accordance with the reported statement that intrinsic wetting thresholds of liquids typically lie around 70°.[23]

With diametrically opposite affinities to liquids with surface tension within the lyophilic (≤ 33.5 mN m^{-1}) and lyophobic (≥ 36.1 mN m^{-1}) regions, a T-ZnO/PLMA-40-coated mesh was expected to be able to reject a liquid in the lyophobic region and allow quick permeation of a liquid in the lyophilic region, hence to separate a mixture of both in a highly efficient manner. Gravity-driven separations of three pairs liquid/liquid mixtures: water/hexadecane (Fig. 4a), [Bmim][BF$_4$]/hexadecane (Fig. 4b) and water/[Hmim][TFSI] (Fig. 4c) were performed through a glass separator (Vid. S1, ESI†), in which the mesh is placed as the filtration layer. The apparatus was inclined when the liquid with higher surface tension was heavier in order to expose the lighter low-surface-energy liquids to the
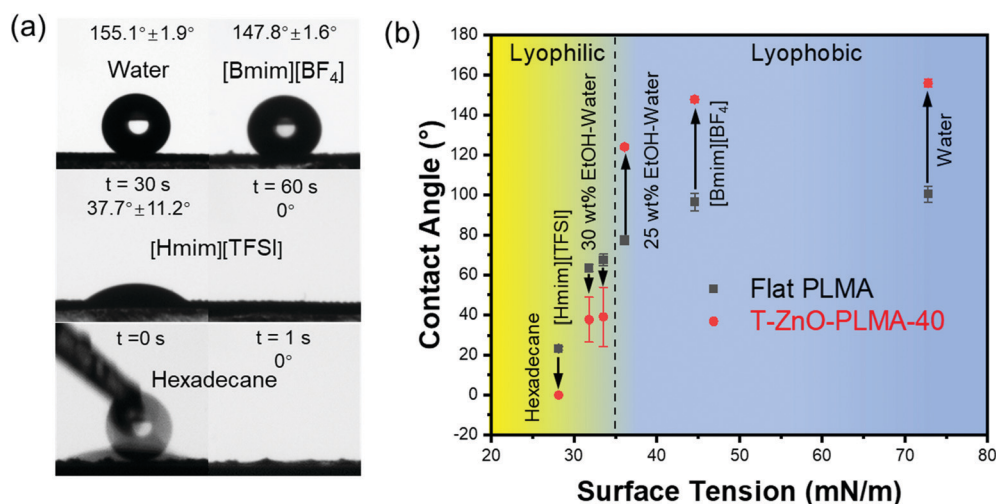

Fig. 3 (a) Contact angles of water, [Bmim][BF$_4$], [Hmim][TFSI], and hexadecane on T-ZnO/PLMA-40. (b) Contact angles of liquids on T-ZnO/PLMA-40 and on smooth PLMA *versus* surface tension. Arrows indicate the wettability amplification from smooth surface to the high-roughness hybrid surface.
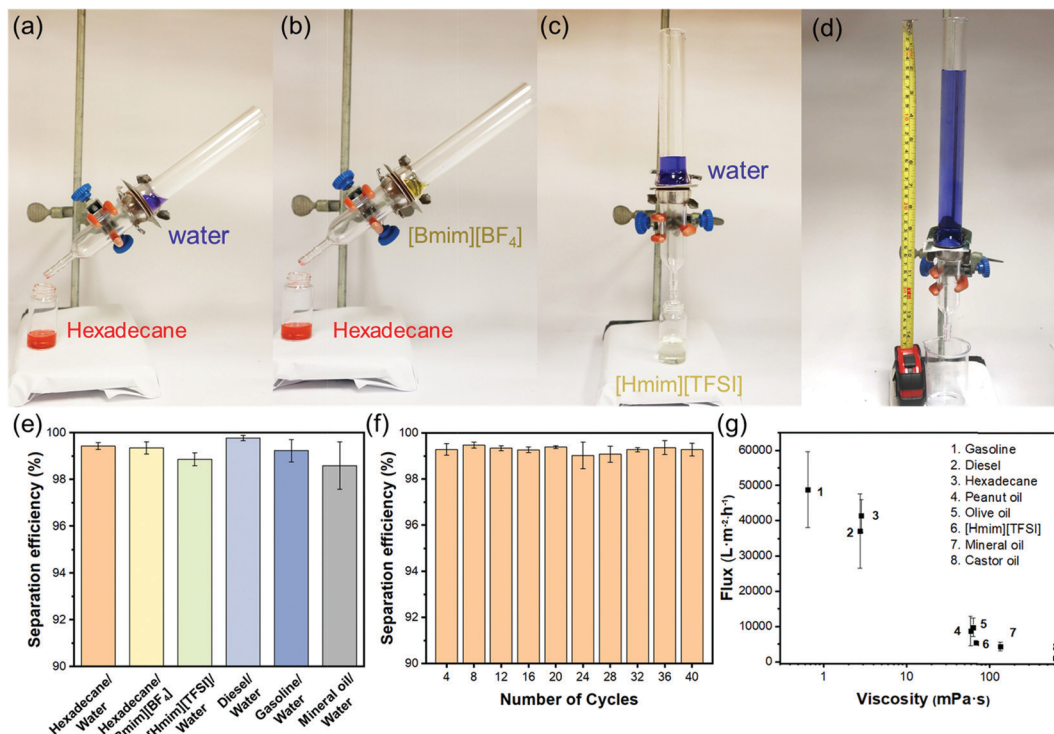
Fig. 4 Separation of (a) water/hexadecane, (b) [Bmim][BF$_4$]/hexadecane, and (c) water/[Hmim][TFSI] by T–ZnO/PLMA-40. Water was dyed with Brilliant Blue R and hexadecane was dyed with Oil O Red. (d) Maximum water intrusion pressure of T–ZnO/PLMA-40. (e) Separation efficiency values of T–ZnO/PLMA-40-coated mesh for six pairs of immiscible liquid/liquid mixtures. (f) Separation efficiency for hexadecane/water mixture after varied numbers of cycles. (g) Fluxes of low-surface-energy liquids permeating the mesh.

membrane and otherwise set perpendicular. As expected, when the mixtures encountered the membrane, the low-surface-energy liquid (oil or [Hmim][TFSI]) permeated quickly while the high surface tension liquid (water or [Bmim][BF$_4$]) retained, enabling the complete separation of the mixtures. The separation efficiencies of the T–ZnO/PLMA-40-coated mesh for six different pairs of immiscible liquid/liquid mixtures (hexadecane/water, hexadecane/[Bmim][BF$_4$], [Hmim][TFSI]/water, diesel/water, gasoline/water and mineral oil/water) were measured to be all above 98% (eqn S2 (ESI†) and Fig. 4e). The separation efficiency for hexadecane/water mixture maintained above 99% after 40 cycles of separation operation (Fig. 4f), demonstrating the excellent durability and reusability of the hybrid coating materials. To evaluate the separation rate, the fluxes of a series of oily liquids were measured (eqn S1 (ESI†) and Fig. 4g). The flux decreased with higher dynamic viscosity, and notably, the flux for gasoline reached up to 48 900 L m^{-2} h^{-1}. The intrusion pressure of rejected water was determined as 1.96 kPa (eqn (S3), ESI†) according to the maximum water column height of 20 cm (Fig. 4d), indicating an outstanding water-resistant property of the superhydrophobic mesh.

Apart from the separation of stratified immiscible liquid/liquid mixtures, it is highly significant yet challenging to separate emulsified liquid/liquid. A much smaller effective pore size of superwettability-based separation membranes is needed in order to separate the much smaller liquid droplets in an emulsion. To demonstrate the capability of separating water-in-oil emulsion using the T–ZnO/PLMA coating, we photochemically applied the coating on quantitative filter papers, which have smaller macropores for separation. A higher amount of T–ZnO (14 mg cm^{-2}) was used to provide a denser superhydrophobic network to reject nanometer sized water droplets. SEM images revealed that a continuous conformal layer of polymer was formed on T–ZnO with macropores in the range of several microns on the top surface of the filter paper (Fig. 5a and b). Meanwhile, the interconnected T–ZnO network constitutes numerous smaller pores with effective pore size <1 μm, which are critical to demulsification and capturing water droplets from emulsions.[59] To test its separation capacity, the T–ZnO/PLMA coated filter paper was used to separate a Span80-stablized water-in-hexane emulsion (2 mg ml^{-1} of surfactant, water : oil (v/v) = 1 : 100). Driven by a mild vacuum pressure (~0.03 MPa), the oil can permeate the filter paper at a high flux of 1343 L m^{-2} h^{-1}, while the water emulsion was apparently removed clearly as observed by naked eye (Fig. 5c and Vid. S2, ESI†). Optical microscopy images demonstrated that the micro-/nanoscale water droplets in hexane could not be observed anymore in the filtrate. The droplet size distribution of the solution before and after the filtration was measured by dynamic light scattering (Fig. 5d). In the feed emulsion, the average water droplet size was 237 nm. In the filtrate, most of the water droplets were smaller than 10 nm, indicating that the majority of the emulsified water droplets were removed efficiently by the T–ZnO/PLMA coated filter paper.
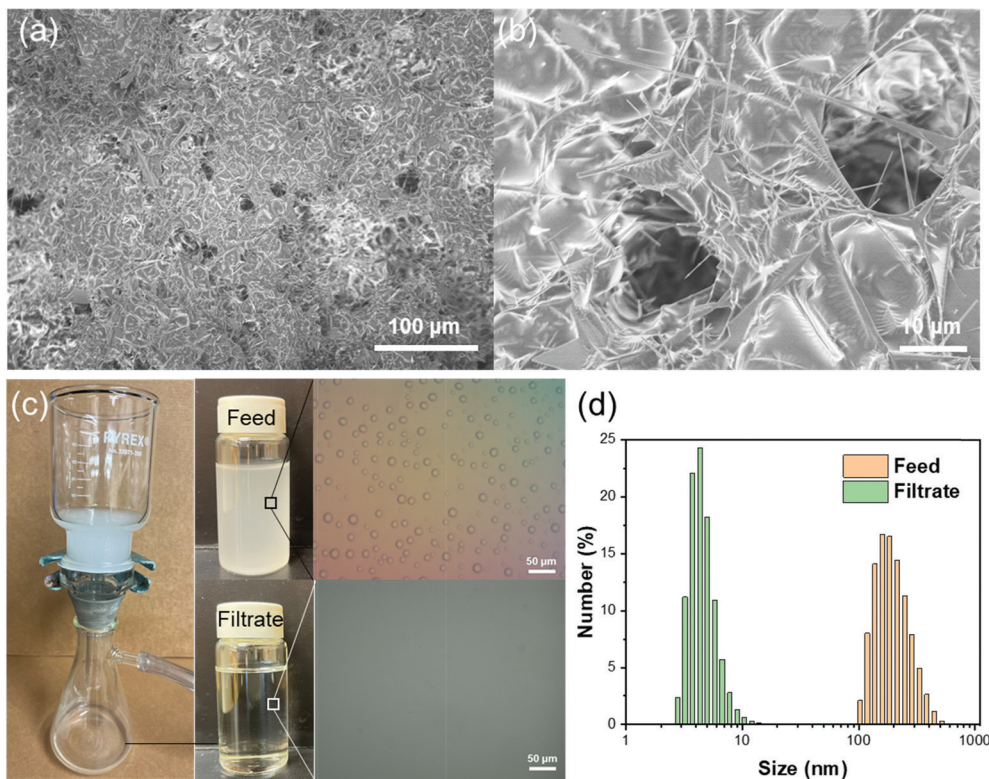
Fig. 5 (a) and (b) SEM images of a T-ZnO/PLMA coated quantitative filter paper. (c) Photographic and optical microscopy images of a surfactant-stabilized water-in-hexane emulsion before and after being filtered through the T-ZnO/PLMA coated filter paper. (d) Normalized water size distribution of the feed and filtrate measured by dynamic light scattering.

Because the superwettability of these materials is directly originated from their surface roughness, the durability of the delicate hierarchically rough structures against various types of environment wear is critical for practical applications.[60] According to our design, the *in situ* polymerized PLMA was generated to cover the surface and to interconnect individual T-ZnO to form an integrated T-ZnO/polymer hybrid layer. The polymer is expected to provide adhesion and protection effects on the local morphology of the T-ZnO spikes. To test this hypothesis, two types of common water impact tests were performed to simulate the liquid impact conditions in liquid/liquid separation applications.[61] In a water drop impact test with 45° tilt angle, it took only tens of drops to sweep away the

T-ZnO on the surface of a control sample without PLMA coating. In comparison, T-ZnO/PLMA-40 exhibited retained WCA of ~155.1° and WSA of 14° after exposure to 100 000 droplets (Fig. 6a). The incorporation of PLMA also enhanced the resistance to water spray as the mesh retained its superhydrophobicity even after 600 cycles (Fig. 6b). As a comparison, the control sample without PLMA coating lost its water repellency within 10 cycles of water spray impact (Vid. S3, ESI†). Both top-view and cross-sectional morphology of T-ZnO/PLMA-40 coated mesh remained almost unchanged after these mechanical tests, except for a slightly flatter surface after the tilted droplets test (Fig. S17 and S18, ESI†). These results suggested good mechanical robustness of the composite coating after T-ZnO is
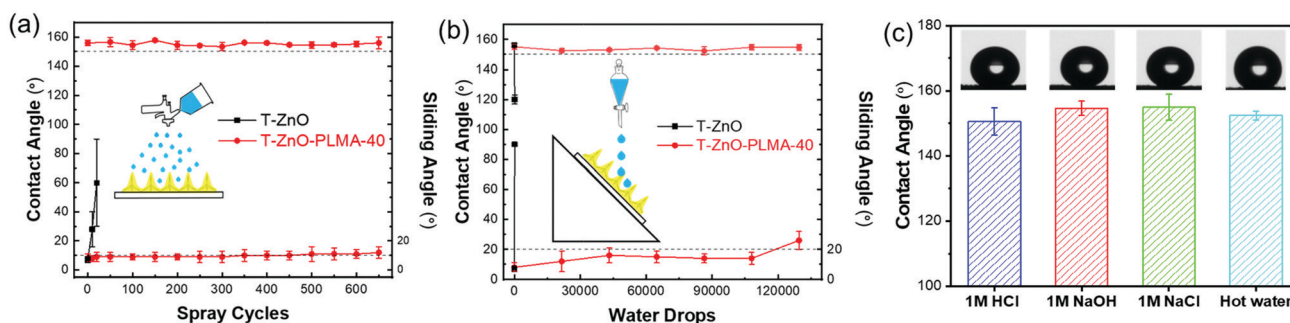

Fig. 6 The durability of T-ZnO coated mesh and T-ZnO/PLMA-40 against (a) water spray impact and (b) water droplet impact. (c) Contact angles of strong acid, base, salt solution, and 70 °C water droplets on T-ZnO/PLMA-40.

wrapped by PLMA, and a slightly better performance in resisting vertical impact than tilted impact. Besides the mechanical impact, harsh chemical and physical environments such as acidic, alkaline, salt solutions and high temperature impose additional potential challenges for many applications. T-ZnO/PLMA-40-coated mesh was tested to separate the mixtures of oil and aqueous 1 M HCl, 1 M NaOH, or 1 M NaCl, all exhibiting fast and clean separation without any notable degradation of the filtration layer (Vid. S4, ESI†). The contact angles of 1 M HCl, 1 M NaOH, 1 M NaCl, and 70 °C hot water droplets on T-ZnO/PLMA-40 were measured to be all above 150° (Fig. 6c), whereas the superhydrophobicity of the bare T-ZnO-coated sample without PLMA deteriorated immediately on exposure to 1 M HCl. This result highlighted the enhanced chemical stability of the composite. Despite the fact that ZnO is highly susceptible to strong acid, the PLMA layer protected it from being in contact with aggressive solutions directly and thus preserved the superhydrophobicity. In addition, PLMA protected the sample from losing its superhydrophobicity against UV irradiation, leading to a much more consistent superhydrophobic performance. For example, the T-ZnO/PLMA-40 coated sample remained superhydrophobic after 2 h of UV irradiation (1 mW cm^{-2}), compared to the complete loss of hydrophobicity of bare T-ZnO after only 1 h of similar irradiation (Fig. S19, ESI†). The significantly improved mechanical, chemical and UV durability of T-ZnO/PLMA-40 enables its potential long-term employment in real-world applications.

One of the critical issues that impedes superwettable coating materials from industrial applications is the challenge to fabricate them in a facile, cost-effective and energy-efficient manner, as most of reported examples require extensive heating.[62] The photopolymerization strategy reported herein holds promises in addressing this issue because heating is not needed throughout the coating process while the chemical and reagents used here are all of low cost. To demonstrate

this potential, a T-ZnO/PLMA-40 coated mesh with a size of 30 cm × 60 cm was prepared (Fig. 7a) by using 10 commercial UV lamps (10 mW cm^{-2}) that are simply assembled parallelly (Fig. S1, ESI†). The resulting large sheet exhibited a uniformly coated surface with excellent water repellent properties (Vid. S5, ESI†). In principle, coated substrates with even larger sizes can be fabricated by simply adding more UV lamps to the set-up, or through roll-to-roll processing. Such photochemical process would be more feasible and energy efficient compared to large-scale processes that require uniform heating.[63–66] Moreover, the photochemical process allows for the coating of superwettable layer on heat-vulnerable substrates, which are deemed impractical for high temperature fabrication methods. As a demonstration, T-ZnO/PLMA-40 was successfully coated onto high-density polyethylene (HDPE, $T_m \sim 132$ °C) and polylactic acid (PLA, $T_g \sim 60$ °C) sheets respectively (Fig. 7b) to render these materials superhydrophobic, without heat-induced deformation or decomposition of the substrate.

Conclusions

We have developed a conceptually new approach to fabricate superhydrophobic/superoleophilic coating materials by taking the advantages of dual functional T-ZnO as the photoinitiator for polymerization meanwhile as the origin of hierarchical surface roughness. The *in situ* photopolymerization of methacrylate monomers was promoted by ZnO in the presence of protic solvent through a hole-oxidation pathway. The super-wettability properties of the resulting ZnO/polymethracrylate was heavily dependent on the type of monomers, the morphology of ZnO, and the amount of polymers formed. The optimized sample, namely, T-ZnO/PLMA-40, showed excellent performance in separating stratified oil/water, oil/IL, and water/IL mixtures, as well as water-in-oil emulsions. The polymethacrylate coating imparted the hybrid with good mechanical robustness under liquid shearing/impact, and resistance against aggressive chemical attacks. The photochemical nature of this method allowed for feaisble large scale fabrication of the coated mesh by using an array of commercial UV lamps, and coating on heat-vulnerable substrate materials. The integration of photopolymerization features, superwettability, and excellent durability renders this hybrid coating approach a highly promising platform technology for various applications.

Conflicts of interest

There are no conflicts to declare.

Acknowledgements

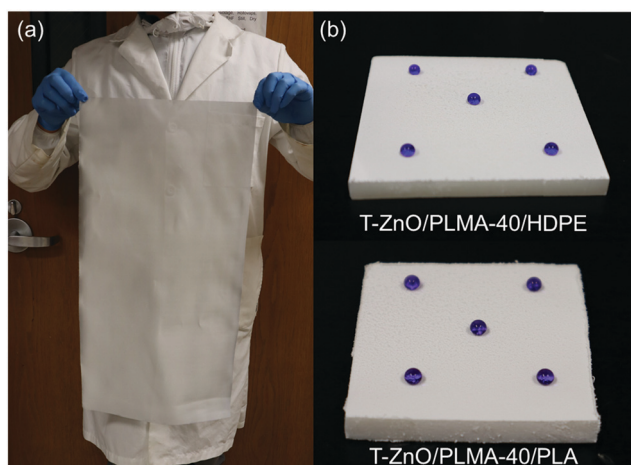**Fig. 7** Photographs of (a) a large size (30 × 60 cm) T-ZnO/PLMA-40 coated mesh; and (b) T-ZnO/PLMA-40 coated HDPE and PLA sheets with dyed blue water droplets.

References

1 J. Chen, Z. Di, J. Shi, Y. Shu, Z. Wan, L. Song and W. Zhang, *J. Cleaner Prod.*, 2020, **273**, 122978.

2 S. A. Northey, G. M. Mudd, T. T. Werner, N. Haque and M. Yellishetty, *Water Resour. Ind.*, 2019, **21**, 100104.

3 T. Ahmad, T. Belwal, L. Li, S. Ramola, R. M. Aadil, Abdullah, Y. Xu and L. Zisheng, *Trends Food Sci. Technol.*, 2020, **99**, 21–33.

4 B. R. Scanlon, R. C. Reedy, F. Male and M. Walsh, *Environ. Sci. Technol.*, 2017, **51**, 10903–10912.

5 C. J. Camphuysen and M. Heubeck, *Environ. Pollut.*, 2001, **112**, 443–461.

6 T. P. Thuy Pham, C.-W. Cho and Y.-S. Yun, *Water Res.*, 2010, **44**, 352–372.

7 N. V. Plechkova and K. R. Seddon, *Chem. Soc. Rev.*, 2008, **37**, 123–150.

8 S. Zhang, J. Sun, X. Zhang, J. Xin, Q. Miao and J. Wang, *Chem. Soc. Rev.*, 2014, **43**, 7838–7869.

9 M. Sato and I. Sumita, *J. Fluid Mech.*, 2007, **591**, 289–319.

10 A. H. Nour, F. S. Mohammed, R. M. Yunus and A. Arman, *Int. J. Chem. Technol.*, 2009, **1**, 59–64.

11 J. L. Diaz de Tuesta, A. M. T. Silva, J. L. Faria and H. T. Gomes, *Chem. Eng. J.*, 2018, **347**, 963–971.

12 Z. Xue, Y. Cao, N. Liu, L. Feng and L. Jiang, *J. Mater. Chem. A*, 2014, **2**, 2445–2460.

13 L. Wang, Y. Zhao, Y. Tian and L. Jiang, *Angew. Chem., Int. Ed.*, 2015, **54**, 14732–14737.

14 C. Chen, D. Weng, A. Mahmood, S. Chen and J. Wang, *ACS Appl. Mater. Interfaces*, 2019, **11**, 11006–11027.

15 L. Feng, Z. Zhang, Z. Mai, Y. Ma, B. Liu, L. Jiang and D. Zhu, *Angew. Chem., Int. Ed.*, 2004, **43**, 2012–2014.

16 A. B. D. Cassie and S. Baxter, *Trans. Faraday Soc.*, 1944, **40**, 546–551.

17 A. B. D. Cassie, *Discuss. Faraday Soc.*, 1948, **3**, 11–16.

18 Y. Si, Q. Fu, X. Wang, J. Zhu, J. Yu, G. Sun and B. Ding, *ACS Nano*, 2015, **9**, 3791–3799.

19 Z. Zhu, W. Wang, D. Qi, Y. Luo, Y. Liu, Y. Xu, F. Cui, C. Wang and X. Chen, *Adv. Mater.*, 2018, **30**, 1801870.

20 X. Q. Cheng, Y. Jiao, Z. Sun, X. Yang, Z. Cheng, Q. Bai, Y. Zhang, K. Wang and L. Shao, *ACS Nano*, 2021, **15**, 3500–3508.

21 J. Zhang and S. Seeger, *Adv. Funct. Mater.*, 2011, **21**, 4699–4704.

22 C. R. Crick, J. A. Gibbins and I. P. Parkin, *J. Mater. Chem. A*, 2013, **1**, 5943–5948.

23 J. Zhang, H. Liu and L. Jiang, *Adv. Funct. Mater.*, 2017, **27**, 1606544.

24 J. Ge, Y.-D. Ye, H.-B. Yao, X. Zhu, X. Wang, L. Wu, J.-L. Wang, H. Ding, N. Yong, L.-H. He and S.-H. Yu, *Angew. Chem., Int. Ed.*, 2014, **53**, 3612–3616.

25 W. Zhang, N. Liu, Y. Cao, Y. Chen, L. Xu, X. Lin and L. Feng, *Adv. Mater.*, 2015, **27**, 7349–7355.

26 X. Bu, Y. Lu, S. Chen, D. Li, Z. Zhang and P. Qian, *Chem. Eng. J.*, 2019, **355**, 299–308.

27 X. Su, H. Li, X. Lai, L. Zhang, J. Wang, X. Liao and X. Zeng, *ACS Appl. Mater. Interfaces*, 2017, **9**, 28089–28099.

28 H. Guo, J. Yang, T. Xu, W. Zhao, J. Zhang, Y. Zhu, C. Wen, Q. Li, X. Sui and L. Zhang, *ACS Appl. Mater. Interfaces*, 2019, **11**, 13704–13713.

29 X. Feng, L. Feng, M. Jin, J. Zhai, L. Jiang and D. Zhu, *J. Am. Chem. Soc.*, 2004, **126**, 62–63.

30 X. Zhang, Z. Li, K. Liu and L. Jiang, *Adv. Funct. Mater.*, 2013, **23**, 2881–2886.

31 C. Wang, T. Yao, J. Wu, C. Ma, Z. Fan, Z. Wang, Y. Cheng, Q. Lin and B. Yang, *ACS Appl. Mater. Interfaces*, 2009, **1**, 2613–2617.

32 Y. Wang, Y. Zhu, C. Yang, J. Liu, W. Jiang and B. Liang, *ACS Appl. Mater. Interfaces*, 2018, **10**, 24149–24156.

33 B. J. M. Velazquez, S. Baskaran, A. V. Gaikwad, T.-T. Ngo-Duc, X. He, M. M. Oye, M. Meyyappan, T. K. Rout, J. Y. Fu and S. Banerjee, *ACS Appl. Mater. Interfaces*, 2013, **5**, 10650–10657.

34 C. Xu, M. Kim, J. Chun and D. E. Kim, *Nanotechnology*, 2005, **16**, 2104–2110.

35 T. E. O'Loughlin, S. Martens, S. R. Ren, P. McKay and S. Banerjee, *Adv. Eng. Mater.*, 2017, **19**, 1600808.

36 T. E. O'Loughlin, R. V. Dennis, N. A. Fleer, T. E. G. Alivio, S. Ruus, J. Wood, S. Gupta and S. Banerjee, *Energy Fuels*, 2017, **31**, 9337–9344.

37 A. Bajpayee, T. E. G. Alivio, P. McKay and S. Banerjee, *Energy Fuels*, 2019, **33**, 5024–5034.

38 Y. Yamauchi, M. Tenjimbayashi, S. Samitsu and M. Naito, *ACS Appl. Mater. Interfaces*, 2019, **11**, 32381–32389.

39 X. Jin, M. Deng, S. Kaps, X. Zhu, I. Hölken, K. Mess, R. Adelung and Y. K. Mishra, *PLoS One*, 2014, **9**, e106991.

40 D. Li, Y. Fan, G. Han and Z. Guo, *Chem. Eng. J.*, 2021, **404**, 126515.

41 A. J. Hoffman, H. Yee, G. Mills and M. R. Hoffmann, *J. Phys. Chem.*, 1992, **96**, 5540–5546.

42 Z. Y. Huang, T. Barber, G. Mills and M. B. Morris, *J. Phys. Chem.*, 1994, **98**, 12746–12752.

43 M. Schmitt, *Nanoscale*, 2015, **7**, 9532–9544.

44 I. Ulku, F. Morlet-Savary, J. Lalevée and H. Yagci Acar, *Polym. Chem.*, 2018, **9**, 828–833.

45 A. Pinkas, N. Waiskopf, S. Gigi, T. Naor, A. Layani and U. Banin, *Nanoscale*, 2021, **13**, 7152–7160.

46 H. M. Xiong, Z. D. Wang and Y. Y. Xia, *Adv. Mater.*, 2006, **18**, 748–751.

47 L. Gao and T. J. McCarthy, *Langmuir*, 2006, **22**, 2966–2967.

48 S. Aprile, E. Del Grosso and G. Grosa, *Xenobiotica*, 2011, **41**, 212–225.

49 H.-M. Xiong, D.-P. Xie, X.-Y. Guan, Y.-J. Tan and Y.-Y. Xia, *J. Mater. Chem.*, 2007, **17**, 2490–2496.

50 M. Shaban, J. Poostforooshan and A. P. Weber, *J. Mater. Chem. A*, 2017, **5**, 18651–18663.

51 S. A. Paniagua, Y. Kim, K. Henry, R. Kumar, J. W. Perry and S. R. Marder, *ACS Appl. Mater. Interfaces*, 2014, **6**, 3477–3482.

52 C. Zhang, M. Cao, H. Ma, C. Yu, K. Li, C. Yu and L. Jiang, *Adv. Funct. Mater.*, 2017, **27**, 1702020.

53 Q. Xu, L. Shen, P. Duan, L. Zhang, F. Fu and X. Liu, *Chem. Eng. J.*, 2020, **379**, 122401.

54 C. Hu, M. Zhao, Q. Li, Z. Liu, N. Hao, X. Meng, J. Li, F. Lin, C. Li, L. Fang, S. Y. Dai, A. J. Ragauskas, H. J. Sue and J. S. Yuan, *ChemSusChem*, 2021, **14**, 4260–4269.

55 H. Taniguchi and K. P. Madden, *Radiat. Res.*, 2000, **153**(447-453), 447.

56 E. A. Vogler, *Adv. Colloid Interface Sci.*, 1998, **74**, 69–117.

57 G. Whyman and E. Bormashenko, *Langmuir*, 2011, **27**, 8171–8176.

58 J. Klomfar, M. Součková and J. Pátek, *J. Chem. Thermodyn.*, 2010, **42**, 323–329.

59 F. Zhang, W. B. Zhang, Z. Shi, D. Wang, J. Jin and L. Jiang, *Adv. Mater.*, 2013, **25**, 4192–4198.

60 W. Zhang, D. Wang, Z. Sun, J. Song and X. Deng, *Chem. Soc. Rev.*, 2021, **50**, 4031–4061.

61 N. Celik, I. Torun, M. Ruzi, A. Esidir and M. S. Onses, *Chem. Eng. J.*, 2020, **396**, 125230.

62 R. K. Gupta, G. J. Dunderdale, M. W. England and A. Hozumi, *J. Mater. Chem. A*, 2017, **5**, 16025–16058.

63 J. Yuan, X. Liu, O. Akbulut, J. Hu, S. L. Suib, J. Kong and F. Stellacci, *Nat. Nanotechnol.*, 2008, **3**, 332–336.

64 Y. Shang, Y. Si, A. Raza, L. Yang, X. Mao, B. Ding and J. Yu, *Nanoscale*, 2012, **4**, 7847–7854.

65 L. Wu, J. Zhang, B. Li and A. Wang, *Polym. Chem.*, 2014, **5**, 2382–2390.

66 Y. Liu, N. Liu, Y. Jing, X. Jiang, L. Yu and X. Yan, *Colloids Surf., A*, 2019, **567**, 128–138.